Biointerface Research in Applied Chemistry
Platinum Open Access Journal (ISSN: 2069-5837)

Article
Volume 11, Issue 1, 2021, 8034 - 8042
https://doi.org/10.33263/BRIAC111.80348042

XRD and FTIR Analysis of Magnesium Substituted Tricalcium Calcium Phosphate Using a Wet Precipitation Method

Asmaa Massit [1], Ahmed El Yacoubi [1], Abdelilah Kholtei [2], Brahim Chafik El Idrissi [1,*]

[1] Laboratory of Advanced Materials and Process Engineering, Faculty of Sciences, Ibn Tofail University, Kenitra, Morocco
[2] Laboratory of Chemistry Biology Applied to Environment, Mouly Ismail University, Faculty of Sciences, BP11201 Meknes, Morocco
* Correspondence: chidrissi@yahoo.fr;

Scopus Author ID 6602822327
Received: 2.06.2020; Revised: 3.07.2020; Accepted: 5.07.2020; Published: 9.07.2020

Abstract: The incorporation of magnesium (Mg) in tricalcium phosphate (TCP) was prepared through a precipitation method followed by calcination at 850 °C in air. Calcium hydroxide, ($Ca(OH)_2$), phosphoric acid, (H_3PO_4), and magnesium chloride ($MgCl_2.6H_2O$) with a Ca/P ratio of 1.5, were mixed as the precursor materials. The concentration of added Mg was varied with respect to calcium (Ca) precursor molarity as such Mg/(Ca +Mg) molar ratio was 0.05, 0.10, and 0.15, while the (Ca+Mg)/P ratio was maintained at 1.50 throughout the experiment. The influence of Mg-doped TCP on phase composition, chemical structure, and a functional group at different weight percentages were accomplished through X-ray diffraction (XRD), inductively coupled plasma optical emission spectroscopy (ICP-OES) and Fourier Transform Infrared Spectroscopy (FTIR) analyses. Based in the results of this research, the presence of magnesium led to the formation of Mg-doped calcium-deficient apatite (MgCDA) at 80°C and Mg-doped β-TCP at 850°C; the incorporation of Mg into the TCP phase causing an expansion of the lattice and increase in the lattice parameter. This result could be considered rather unusual.

Keywords: Tricalcium phosphate; Magnesium; precipitation method; XRD and FTIR.

1. Introduction

Hydroxyapatite ($Ca_{10}(PO_4)_6(OH)_2$, HA) and β-tricalcium phosphate (β-TCP, β-$Ca_3(PO_4)_2$) have been considered the most promising materials for both dental and orthopedic applications, because of their chemical similarity to that of human hard tissue [1-5]. Owing to their favorable biological response, these materials have been applied in a wide range of typologies like cement [6,7]. Nevertheless, their applications are limited due to some disadvantages. For example, HA shows a limited ability to stimulate the development of new bone tissue and does not degrade significantly [8]. The weak mechanical properties of β-TCP ceramics, due to its brittleness and insufficient compaction, are limiting its use to non-load-bearing applications.

The most thoroughly investigated material considering ionic substitution is β-TCP [9-13]. In turn, magnesium is definitely the most widely incorporated dopant into its crystal lattice [14-16]. Magnesium (Mg) ion is an essential trace element where it is the fourth cation in the human body that plays an important role in preventing osteoporosis and increase the

regeneration of bone in biomedical applications. Generally, the magnesium content in the human body is known between 0.5 to 1.5wt% [17-20]. Bone contains 0.72wt% of magnesium that are required in the growth of osteoblast and osteoplastic activity of the bone. Mg and Ca provide strong and healthy bones and reduce osteoporosis. Osteoporosis happens due to the high content of calcium with low content of magnesium that affects the fracture of bone [21]. Also, doping β-TCP with Mg ions decreases its solubility [22]. Synthesis methods, such as precipitation [23,24], wet mixing [25,26], mechanochemical-hydrothermal synthesis [27,28], in-situ synthesis [29], solid-state reactions [30,31], sol-gel [32,33] and room temperature synthesis method [34] have been applied. The preparation of TCP through aqueous precipitation usually involves the synthesis of calcium-deficient apatite (CDA) by adjusting the initial Ca/P molar ratio of the precursors to 1.50 and subsequent calcination in the range of 700-800°C to form TCP with the loss of water as represented in the equation (1) :

$$Ca_9(HPO_4)(PO_4)_5OH \rightarrow 3Ca_3(PO_4)_2 + H_2O$$

However, there are very few studies available in the literature on the synthesis and characterization of tricalcium calcium phosphate-containing magnesium prepared via the wet precipitation method. In this work, precursor materials that are normally used to synthesize hydroxyapatite (HA) directly were adopted to obtain β-TCP and Mg-βTCP. The influence of the Mg substitution in the lattice parameters of the unit cell β-TCP was evaluated.

2. Materials and Methods

Tricalcium phosphate and Mg-substituted tricalcium phosphate with Mg/(Ca+Mg) ratio equal to 0 (TCP0), 0.05 (TCP1), 0.10 (TCP2) and 0.15 (TCP3) were synthesized by precipitation method [35] from an aqueous solution of calcium hydroxide [$Ca(OH)_2$] (Scharlau, Spain) orthophosphoric acid [H_3PO_4] (Riedel-de Haën, 85%) and magnesium chloride [$MgCl_2.6H_2O$] (Riedel-de Haën, Germany) at 40°C, pH = 9 (concentrations of the precursors are depicted in Table 1). A predetermined concentration of $MgCl_2.6H_2O$ was added slowly to the continuously stirred solution of $Ca(OH)_2$. The aqueous solution of H_3PO_4 was added rapidly to the above solution containing calcium and Magnesium ions using a vigorous stirring. According to Table 1, the nominal composition, in terms of (Ca+Mg)/P ratio, was maintained at 1.50. Precipitates were aged in mother liquors at room temperature for 24 h, washed with distilled water, vacuum filtered, and finally dried 24h in an oven at 80°C. The dried samples were further calcined 12h at 850°C. In the case of the Mg-TCP precursor, it has been assumed that magnesium ions would substitute for the calcium site in the apatite lattice.

Table 1. Molar concentrations of the precursors Ca, P, and Mg used in the synthesis.

Sample code	Molar Concentrations			Ca/P ratio	(Ca + Mg)/P ratio
	Ca	P	Mg		
TCP0	0.600	0.400	0.000	1.50	1.50
TCP1	0.570	0.400	0.030	1.42	1.50
TCP2	0.540	0.400	0.060	1.35	1.50
TCP3	0.510	0.400	0.090	1.27	1.50

X-ray diffraction characterization of all batches of as-prepared and calcined Mg-TCP powders was performed using Cu Kα radiation. Samples were analyzed over a 2θ range of 10–80° with a sampling interval of 0.07° (XRD, Kristalloflex D-500, Siemens Analytical X-ray Instrument Inc., Madison, WI). Crystallographic identification of the synthesized phases was accomplished by comparing the experimental XRD patterns to standards compiled by the Joint

Committee on Powder Diffraction and Standards (JCPDS), which were card #09- 0169 for TCP (a=10.432(3)A˚, b=10.432(3)A˚, c=37.39A˚, space group *R*3*c* (167), theoretical density 3.072g/cm^3, V =3520.91A˚^{3}, Z= 21) and #33-0297 for β-$Ca_2P_2O_7$.

The average crystallite size D(hkl) in nm was estimated following Debey–Scherrer equation [30]:

$$Dhkl = \frac{k\lambda}{\beta cos\theta}$$

where K is the shape factor equal to 0.9, λ is the X-rays wavelength (equal to 1.5406 A˚ for Cu Ka radiation), θ is the Bragg's diffraction angle (in degrees), and β is the full width at half maximum (FWHM). The diffraction peak at 25.88 (2θ) corresponding to (0 0 2) Miller plane family of apatite lattice (JCPDS file #09-0432), was chosen to calculate the average crystal size along to the crystallographic axis c. The length of coherent domains D(2 0 10) in TCP crystallites was also calculated using the line broadening of the (2 0 10) peak (diffraction angle 2θ (31.08°)) [36], applying the Scherrer's equation to XRD spectra of samples calcined at 850°C.

Cell parameters of the tricalcium phosphate phase were estimated through the algorithm DICVOL 06 (Fullprof-suite software), using XRD diffraction patterns of samples calcined.

The chemical structure of powders was evaluated in the vibration range of 400–4000 cm^{-1}, using an Infrared Fourier Spectrometer (VERTEX 70, Genesis Series, resolution 4, scans 20). For this, 1% of the powder was mixed and ground with 99% KBr.

3. Results and Discussion

XRD patterns of all as-prepared TCP and Mg-TCP powders are compared in Figure 1. All samples showed the typical diffraction pattern of the calcium-deficient hydroxyapatite (CDA) as from the perfect match with HA (#09-0432 card) characteristic reflections. In the pure TCP and the Mg-TCP samples, no other XRD peaks except for those derived from the CDA phase were observed. The substitution of Mg did not appear to affect the diffraction patterns of the as-prepared powders. Moreover, due to the existence of Mg, the diffraction peaks slightly shifted to larger angles in the pattern (figure 2), indicating the incorporation of Mg into β-TCP.

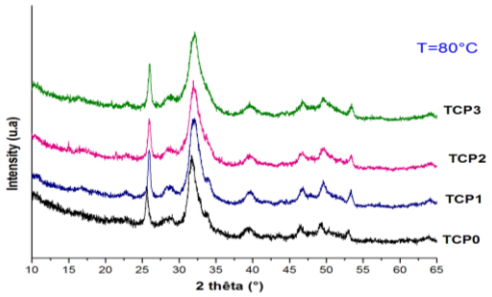

Figure 1. XRD patterns of as-dried TCP and Mg-TCP precursors.

With increasing the amount of Mg in calcium-deficient apatite, the crystallinity of the apatite phase gradually decreased as manifested by the increased broadening of their XRD peaks. The gradual decrease of crystallinity is one of the indications suggesting increasing Mg incorporation in the CDA lattice. The calculated crystallite sizes are 25.5 nm (TCP0), 22.4 nm (TCP1), 20.7 nm (TCP2), and 20.5 nm (TCP3), respectively. The presence of Mg^{2+} ions seems to make the crystallization more difficult, as also observed in previous works for MgTCP powders [31, 37]. CDA powders are produced according to the reaction (1):

$$(9\text{-}3x)Ca(OH)_2 + 6H_3PO_4 + 3xMgCl_2.6H_2O \rightarrow Ca_{(9-3x)}Mg_{3x}(HPO_4)(PO_4)_5(OH) + 6xHCl + (17 + 12x)H_2O$$

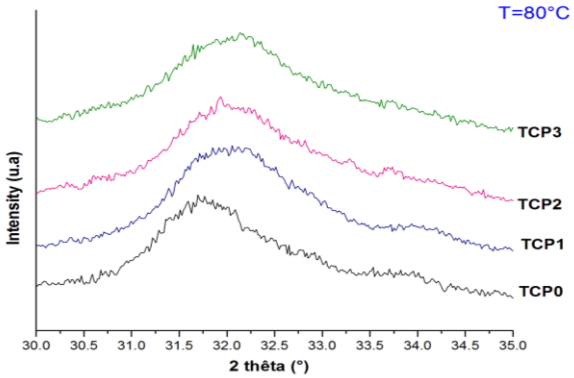

Figure 2. X-ray diffraction showing peak shifts to larger angles after incorporation of Mg.

It is important to underline that TCP cannot be synthesized directly in aqueous solution by the wet method. The precipitate is an apatitic tricalcium phosphate $Ca_9(HPO_4)(PO_4)_5(OH)$, consisting of calcium-deficient hydroxyapatite, $Ca_{10}(PO_4)_6(OH)_2$ where HPO_4^{2-} ion partially substitutes the PO_4^{3-} groups. The crystallization of anhydrous β-TCP requires further calcination of the apatitic compound at temperatures over 750°C [38]. For this reason, it is essential to carry out X-ray diffraction analysis on samples that have been heating treated at temperatures higher than 750°C in order to assess the effect of chemical changes on the phase composition and formation of pure β-tricalcium phosphate with Mg incorporation in its structure.

ICP was adopted to evaluate the actual Mg-doped amounts of the samples (TCP0, TCP1, TCP2, and TCP3). As shown in Table 2, the actual Mg-doped amounts of all the samples were closed to the designed ratios, but all were a little higher than that. Ca(4) in β-TCP has a lower occupancy factor of 0.43(4) [39]. Because of the shorter distance of Mg–O, after Mg is replaced with Ca, it altered the crystal lattice, which may intensify the vacancy of Ca ions, leading to the increase in Mg/(Ca+Mg) ratio.

Table 2. Molar ratio of (Ca+Mg)/P and Mg/(Ca + Mg) of the samples.

Samples	(Ca+Mg)/P	Mg/(Ca+Mg)
TCP0	1.501	0
TCP1	1.496	5.813%
TCP2	1,478	11.744%
TCP3	1.488	15.124%

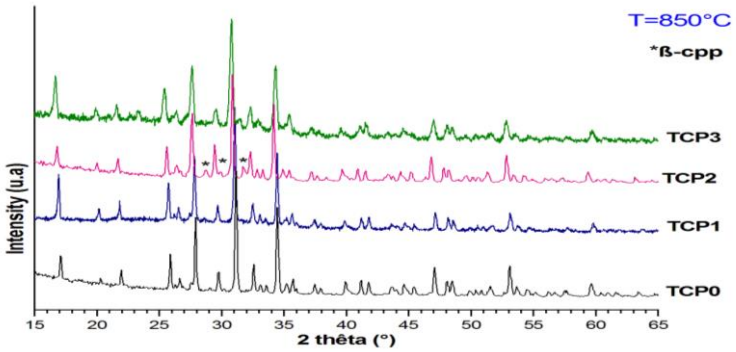

Figure 3. XRD spectra of the TCP Mg-TCP precursors calcined at 850°C.

The XRD profiles (figure 3) of calcined undoped and Mg-doped CDA powders showed that all the calcined samples were completely transformed to β-TCP and Mg-β-TCP, respectively, according to equation (2):

$$Ca_{(9-x)}Mg_x(HPO_4)(PO_4)_5(OH) \rightarrow 3(Ca_{3-(x/3)}Mg_{x/3})(PO_4)_2 + H_2O$$

In these powders, the precursors (Ca+Mg)/P molar ratio during synthesis was adjusted to 1.50 to ensure the incorporation of Mg into β-TCP. In the Mg-TCP samples with Mg/(Ca+Mg) = 0.05 and 0.15 (TCP1 and TCP3 samples), no other XRD peaks except for those derived from the TCP phase were observed, while peaks indicating the presence of $Ca_2P_2O_7$ (β-CPP) were observed in the sample with Mg/(Ca+Mg) = 0.10 (TCP2). When analyzing the vibrational bands of the samples doped with Mg^{2+}, as observed in Figure 3, we realized that there were substitutions in the connection sites with phosphate, which would release Ca^{2+} ions and affect the chemical composition of the material, leading to the formation of new phases. Then, the substitution of Ca^{2+} by Mg^{2+} occurred at these sites and decreased the Ca/P ratio by changing the crystalline structure of β-TCP to β-CPP. With increasing Mg substitution, the XRD peaks became gradually broader and weaker. This effect could be explained by decreased crystallite size and increased lattice disorder associated with increasing Mg substitution in the TCP lattice. Peak positions shift to lower angles and are also observed (figure 4), which indicates lattice expansion caused by magnesium substitution. These observed peaks shift in the XRD pattern is a clear indication of the incorporation of Mg into the TCP phase, causing an expansion of the lattice and an increase in the lattice parameter. This could be considered somewhat unusual since Mg^{2+} is smaller in size (ionic radius ~0.65Å) compared to Ca^{2+} (ionic radius ~0.99Å). There are five crystallographically independent sites, Ca(1)-Ca(5), in the unit cell of β-TCP [40], but Ca^{2+} can be replaced by Mg^{2+} only on Ca(4) and Ca(5) sites in the β-TCP structure. According to Enderle et al. [41], the Ca^{2+} up to 10 mol% Mg^{2+} is preferably replaced on the six-fold coordinated Ca(5) site resulting in a decrease of both lattice parameters. Replacement of Ca^{2+} on the nine-fold coordinated Ca(4) site by Mg^{2+} does not significantly take place until the Ca(5) site is completely occupied by Mg^{2+}. Above 10 mol% replacement by Mg^{2+}, the nine-fold coordinated Ca(4) site is occupied by Mg^{2+}, and the lattice parameters increase until maximum substitution. Hence the Mg^{2+} may be probably occupying an interstitial site rather than an actual lattice site causing increase cell parameter a.

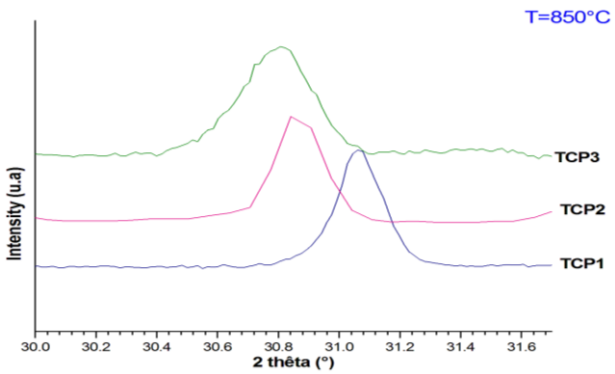

Figure 4. X-ray diffraction showing peak shifts after Mg is substituted indicative of lattice expansion.

Calculated cell parameters are reported in Table 3. An increase of 'a' and 'c' was detected. Finally, the mean crystallite size of pure TCP and Mg-TCP precursors calcined at

850°C, i.e., TCP0, TCP1, TCP2, and TCP3 was estimated as about 47.1 nm, 46.7 nm, 42.9 and 31.9 nm, respectively.

Table 3. Calculated cell parameters of β -Mg- substituted tricalcium phosphate calcined at 850°C.

Sample	Mg/(Ca+Mg)	a(A°)	c(A°)	V (A°3)
TCP0	0	10.402(4)	37.293(5)	3495
TCP1	0.05	10.412(4)	37.403(2)	3511
TCP2	0.10	10.427(7)	37.415(8)	3522
TCP3	0.15	10.440(5)	37.424(3)	3532

The FTIR analysis (Figure 5) of the as-prepared CDA and Mg-CDA powders was in good accordance with the results of the XRD analysis. Selected FTIR spectra to show the characteristic bands of Ca deficient apatite groups: ν4 PO_4^{3-} (560–600 cm^{-1}), ν1 PO_4^{3-} (960 cm^{-1}), and ν3 PO_4^{3-} (1020–1120 cm^{-1}). The band at 875 cm^{-1} is ascribed to HPO_4^{2-} stretching mode of hydrogen phosphate groups. The very weak peaks located at 630 cm^{-1} and 3568 cm^{-1} were attributed to OH^-. The amount of carbonate detected at 1420 and 1456 cm^{-1}. The presence of functional groups such as OH^-, HPO_4^{2-} and PO_4^{3-} confirms that the powders prepared and then dried at 80°C are only DCA and Mg-DCA structures.

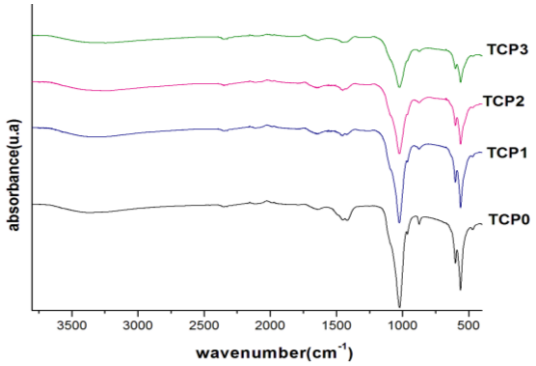

Figure 5. FTIR spectra of as-dried TCP and Mg-TCP precursors.

The FTIR spectra of TCP and Mg-TCP precursors calcined at 850°C are presented in Figure 6. As can be seen, the FTIR results of magnesium substituted tricalcium phosphate indicate the typical peaks characteristic of pure β-TCP [42]. The infrared absorption bands located at 1132, 1030, 990, 960, 610, and 560 cm^{-1} contribute to the confirmation of PO_4 tetrahedra of β-$Ca_3(PO_4)_2$ structure [43]. The TCP2 sample showed additional peaks at 756 and 1213 cm^{-1} ascribed to the symmetrical stretching vibration of the P–O–P group, which is characteristic of the calcium pyrophosphate phase $Ca_2P_2O_7$ in agreement with the previous XRD results.

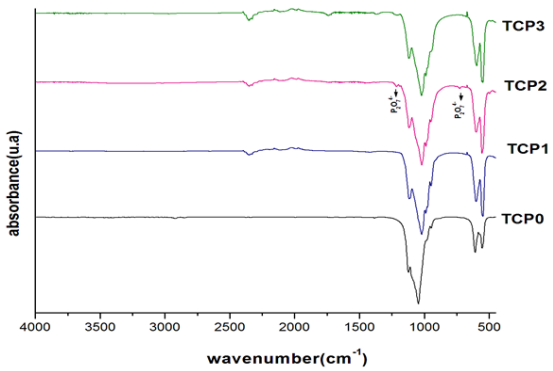

Figure 6. FTIR spectra of TCP and Mg-TCP precursors calcined at 850°C.

4. Conclusions

Pure and Mg-doped calcium phosphate compounds were synthesized via the precipitation method starting from $Ca(OH)_2$, H_3PO_4, and $MgCl_2.6H_2O$. The thermal behavior at 80°C and 850°C of synthesized powders were studied with the help of FTIR and XRD data. Based on the results of this research, nanosized phase β-Mg-TCP powders were obtained by thermal treatment at 850°C. The crystallite size of Mg-CDA decreased with increasing Mg^{2+} content. It could be observed that both the cell parameters and cell volume increase, unusually, with Mg content.

Funding

This research received no external funding.

Acknowledgments

This research has no acknowledgment.

Conflicts of Interest

The authors declare no conflict of interest.

References

1. Kannan, S.; Goetz-Neunhoeffer, F.; Neubauer, J.; and Ferreiraw, J.M.F. Ionic substitutions in biphasic hydroxyapatite and β-tricalcium phosphate mixtures: structural analysis by rietveld refinement. *J. Am. Ceram. Soc* **2008**, *91*, 1–12, https://doi.org/10.1111/j.1551-2916.2007.02117.x.
2. Jorge, E.; Chanfrau, R. Evaluation of the influence of microwave irradiation on a bacterial composed of three phases of calcium phosphates. *Biointerface Research in Applied Chemistry* **2020**, *10*, 5141-5144, https://doi.org/10.33263/BRIAC102.141144.
3. Jorge, E.; Chanfrau, R.; Yaymarilis, V.P.; Antonio, C.G. Ultrasonic Application and spry drying during amorphous calcium phosphate synthesis. *Letters in Applied NanoBionScience* **2019**, *8*, 711-714, https://doi.org/10.33263/LIANBS84.711714.
4. Ruiz-Aguilar, C.; Olivares-Pinto, U.; Drew, R.A.L.; Aguilar-Reyes, E.A.; Alfonso, I. Porogen Effect on Structural and Physical Properties of *β*-TCP Scaffolds for Bone Tissue Regeneration. *IRBM* **2020**, (In Press). https://doi.org/10.1016/j.irbm.2020.05.007.
5. Gallo, M.; Tadier, S.; Meille, S.; Chevalier, J. Resorption of calcium phosphate materials: considerations on the in vitro evaluation. *Journal of the European Ceramic Society* **2018**, 38, 3, 899-914, https://doi.org/10.1016/j.jeurceramsoc.2017.07.004.
6. Fathi, M.; Kholtei, A.; EL Youbi, S.; Chafik El Idrissi, B. Setting Preperties of Calcium Phosphate Bone Cement. *Materials Today: Proceedings* **2019**, *13*, 876-881, https://doi.org/10.1016/j.matpr.2019.04.051.
7. Fathi, M.; Massit, A.; El Yacoubi, A.; Chafik El Idrissi, B. Development of an apatitic calcium phosphate cements: effect of liquid/poder ratio on the setting time. *Mor. J. Chem* **2020**, *8*, 176-183.
8. Bianco, A.; Cacciotti, I.; Lombardi, M.; Montanaro, L. Si-substituted hydroxyapatite nanopowders: Synthesis, thermal stability and sinterability. *Materials Research Bulletin* **2009**, *44*, 345-354, https://doi.org/10.1016/j.materresbull.2008.05.013.
9. Boanini, E.; Gazzano, M.; Nervi, C.; Chierotti, M.R.; Rubini, K.; Gobetto, R.; Bigi, A. Strontium and Zinc Substitution in β-Tricalcium Phosphate: An X-ray Diffraction, Solid State NMR and ATR-FTIR Study. *J. Funct. Biomater* **2019**, *10*, https://doi.org/10.3390/jfb10020020.
10. Altomare, M.; Rizzi, R.; Rossi, M.; El Khouri, A.; Elaatmani, M.; Paterlini, V.; Ventura, G. D.; F. Capitelli. New $Ca_{2.90}(Me^{2+})_{0.10}(PO_4)_2$ β-tricalcium Phosphates with Me^{2+} = Mn, Ni, Cu: Synthesis, Crystal-Chemistry, and Luminescence Properties, *Crystals* **2019**, *9*, https://doi.org/10.3390/cryst9060288.
11. Tkachenko, S.; Horynová, M.; Casas-Luna, M.; Diaz-de-la-Torre, S.; Dvořák, K.; Celko, L.; Kaiser, J.; Montufar, E.B. Strength and fracture mechanism of iron reinforced tricalcium phosphate cement fabricated by spark plasma sintering. *J. Mech. Behav. Biomed. Mater.* **2018**, *81*, 16–25, https://doi.org/10.1016/j.jmbbm.2018.02.016.
12. Sinusaite, L.; Renner, A.M.; Schütz, M.B.; Antuzevics, A.; Rogulis, U.; Grigoraviciute-Puroniene, I.; Mathur, S.; Zarkov, A. Effect of Mn doping on the low-temperature synthesis of tricalcium phosphate (TCP)

polymorphs. *Journal of the European Ceramic Society* **2019**, *39*, 3257-3263, https://doi.org/10.1016/j.jeurceramsoc.2019.03.057.
13. Aurélie, J.; Gaulier, M.; Duval, A.; Renaudin, R. Silver Doping Mechanism in Bioceramics-From Ag^{+}:Doped HAp to Ag°/BCP Nanocomposite. *Crystals* **2019**, *9*, https://doi.org/10.3390/cryst9070326.
14. Nikaido, T.; Tsuru, K.; Munar, M.; Maruta, M.; Matsuya, S.; Nakamura, S.; Ishikawa, K. Fabrication of β-TCP foam: Effects of magnesium oxide as phase stabilizer on its properties. *Ceramics International* **2015**, *41*, 14245-14250, https://doi.org/10.1016/j.ceramint.2015.07.053.
15. Salma-Ancane, A.; Stipniece, L.; Putnins, A.; Berzina-Cimdina, L. Development of Mg-containing porous β-tricalcium phosphate scaffolds for bone repair. *Ceram. Int* **2015**, *41*, 4996–5004. https://doi.org/10.1016/j.ceramint.2014.12.065.
16. Frasnelli, M.; Pedranz, A.; Biesuz, M.; Dirè, S.; Sglavo, V.M. Flash sintering of Mg-doped tricalcium phosphate (TCP) nanopowders. *Journal of the European Ceramic Society* **2019**,*39*, 3883–3892, https://doi.org/10.1016/j.jeurceramsoc.2019.05.007.
17. García-Páez, H.; García Carrodeguas, R.; De Aza, A.H.; Baudín, C.; Pena, P. Effect of Mg and Si co-substitution on microstructure and strength of tricalcium phosphate ceramics. *J. Mech. Behav. Biomed. Mater* **2014**, 30, 1–15, https://doi.org/10.1016/j.jmbbm.2013.10.011.
18. Adzila, S.; Kanasan, N.; Fahrul, M.; Mubarak, A.; Arifin, T.; Nasrull, M, & Rahman, A. Synthesis and characterization of magnesium doped calcium phosphate for bone implant application. *J. ofEng. and Appl. Sci* **2016**, *11*, 1819-6608.
19. Nanthini, K.; Adzila, S.; Suid, M.S.; Panerselvan, G. Preparation and Characterization of Hydroxyapatite/Sodium Alginate Biocomposites for Bone Implant Application. *AIP Proceedings* **2016,** *1756*, 5162–5165, https://doi.org/10.1063/1.4958749.
20. Kanasan, N.; Adzila, S.; Azimahmustaffa, N.; Gurubaran, P. The Effect of Sodium Alginate on the Properties of Hydroxyapatite. *Procedia Engineering* **2017** , *184*, 442-448, https://doi.org/10.1016/j.proeng.2017.04.115.
21. Kanasan, N.; Adzila, S.; Rahman, H.A.; Bano, N.; and Panerselvan, G.; Hidayati, N.A. FTIR and XRD Evaluation of Magnesium Doped Hydroxyapatite/Sodium Alginate Powder by Precipitation Method. *Key Engineering Materials* **2018**, *791*, 45-49, https://doi.org/10.4028/www.scientific.net/KEM.791.45.
22. Gallo, M.; Le Gars Santoni, B.; Douillard, T.; Zhang, F.; Gremillard, L.; Dolder, S.; Hofstetter, W.; Meille, S.; Bohner, M.; Chevalier, J.; Tadier, S.; Hofstetter, W.;Meille, S.; Bohner, M.; Chevalier, J.; Tadier, S. Effect of grain orientation and magnesium doping on β-tricalcium phosphate resorption behavior. *Acta Biomaterialia* **2019**, *89*, 391-402, https://doi.org/10.1016/j.actbio.2019.02.045.
23. Sader, M.S.; Legeros, R.Z.; Soares, G.A. Human osteoblasts adhesion and proliferation on magnesium-substituted tricalcium phosphate dense tablets. *J. Mater. Sci. Mater. Med* **2009**, *20*, 521–527, https://doi.org/10.1007/s10856-008-3610-3.
24. Kubarev, O.L.; Barinov, S.M.; Komlev, V.S. Magnesium distribution in the synthesis of biphasic calcium phosphates. *Dokl. Chem* **2008**, *418*, 44–46, https://doi.org/10.1134/S0012500808020067.
25. Zyman, Z.; Tkachenk, M.; Epple, M.; Polyakov, M.; Nabok M. Magnesium-substituted hydroxyapatite ceramics. *Mat. wiss. u. Werkstofftech* **2006**, *37*, 474–478, https://doi.org/10.1002/mawe.200600022.
26. Tan, C.Y.; Aw, K.L.; Yeo, W.H.; Ramesh, S.; Hamdi, M, Sopyan, I. Influence of magnesium doping in hydroxyapatite ceramics. *Biomed*. **2008** , *21*, 326–329, https://doi.org/10.1007/978-3-540-69139-6_83.
27. Suchanek, W.L.; Byrappa, K.; Shuk, P.; Riman, R.E. Preparation of magnesium-substituted hydroxyapatite powders by the mechanochemical–hydrothermal method. *Biomaterials* **2004**, *25*, 4647-4657, https://doi.org/10.1016/j.biomaterials.2003.12.008.
28. Suchanek, W.L.; Byrappa, K.; Shuk, P.; Riman, R.E.; Janas, V.F, TenHuisen, K.S. Mechanochemical–hydrothermal synthesis of calcium phosphate powders with coupled magnesium and carbonate substitution. *J. Solid State Chem.* **2004**, *177*, 793–799, https://doi.org/10.1016/j.jssc.2003.09.012.
29. Lee, D.; Sfeir, C.; Kumta, P.N. Novel in-situ synthesis and characterization of nanostructured magnesium substituted *β*-tricalcium phosphate *β*-TCMP. *Mater. Sci. Eng. C.* **2009**, *29*, 69–77, https://doi.org/10.1016/j.msec.2008.05.017.
30. Tardei, C.; Grigore, F.; Pasuk, I.; Stoleriu, S. The study of Mg^{2+}/Ca^{2+} substitution of β-tricalcium phosphate. *J. Optoelectron. Adv. Mater.* **2006**, *8*, 568–571.
31. Frasnelli, M.; Sglavo, V.M. Effect of Mg^{2+} doping on β-α phase transition in tricalcium phosphate ceramics. *Acta Biomater*. **2016**, *33*, 283-9, https://doi.org/10.1016/j.actbio.2016.01.015.
32. Ruiz-Aguilar, C.; Olivares-Pinto, U.; Aguilar-Reyes, E.A.; López-Juárez, R.; Alfonso, I. Characterization of β-tricalcium phosphate powders synthesized by sol–gel and mechanosynthesis. *Boletín de la Sociedad Española de Cerámica y Vidrio* **2018**, *57*, 213-220, https://doi.org/10.1016/j.bsecv.2018.04.004.
33. Gozalian, A.; Behnamghader, A.; Daliri, M.; Moshkforoush, A. Synthesis and thermal behavior of Mg-doped calcium phosphate nanopowders via the sol gel method. *Scientia Iranica F0* **2011**, *18*, 1614–1622, https://doi.org/10.1016/j.scient.2011.11.014.
34. Liu, L.; Wu, Y.; Xu, C.; Suchun Yu.; Wu, X.; Dai, H. Synthesis, Characterization of Nano-***β***-Tricalcium Phosphate and the Inhibition on Hepatocellular Carcinoma Cells. *Journal of Nanomaterials* **2018**, *2018*, https://doi.org/10.1155/2018/7083416.

35. Massit, A.; El Yacoubi, A.; Rezzouk, A.; Chafik El Idrissi, B. Thermal Behavior of Mg-Doped Calcium-Deficient Apatite and Stabilization of β Tricalcium Phosphate.. *Biointerface Research in Applied Chemistry* **2020**, 10, *6*, 6837-6845.
36. Cacciotti, I.; Bianco, A. High thermally stable Mg-substituted tricalcium phosphate via precipitation, *Ceramics International*. **2011**, *37*, 127–137, https://doi.org/10.1016/j.ceramint.2010.08.023.
37. Frasnelli, M.; Pedranz, A.; Biesuz, M.; Dirè, S.; Sglavo, V.M. Flash sintering of Mg-doped tricalcium phosphate (TCP) nanopowders. *Journal of European Ceramic societ.* **2019**, *39*, 3883-3892, https://doi.org/10.1016/j.jeurceramsoc.2019.05.007.
38. Destainville, A.; Champion, E.; Bernache-Assollant, D.; La Borde, E. Synthesis, characterization and thermal behaviour of apatitic tricalcium phosphate.*Mater. Chem. Phys.* **2003**, *80*, 269–277, https://doi.org/10.1016/S0254-0584(02)00466-2.
39. Guo, X.; Long,Y.; Li, W.; Dai, H. Osteogenic effects of magnesium substitution in nanostructured b-tricalcium phosphate produced by microwave synthesis. *J Mater Sci* **2019**, *54*, 11197–11212, https://doi.org/10.1007/s10853-019-03674-7.
40. Yashima, M.; Sakai, A.; Kamiyama, T.; Hoshikawa, A. Crystal structure analysis of *β*-tricalcium phosphate $Ca_3(PO_4)_2$ by neutron powder diffraction. *J. Solid State Chem* **2003**, *175*, 272-277, https://doi.org/10.1016/S0022-4596(03)00279-2.
41. Enderle, R.; Gotz-Neunhoeffer, F.; Gobbels, M.; Muller, F.A.; Greil, P. Influence of magnesium doping on the phase transformation temperature of β-TCP ceramics examined by Rietveld refinement. *Biomaterials* **2005**, *26*, 3379–3384. https://doi.org/10.1016/j.biomaterials.2004.09.017.
42. Fathi, M.; El Yacoubi, A.; Massit, A.; Chafik El Idrissi, B. Wet chemical method for preparing high purity β and α-tricalcium phosphate crystalline powders. *Int J Sci Eng Res* **2015**, *6*, 139-142.
43. Massit, A.; Fathi, M.; El Yacoubi, A.; Kholtei, A.; Chafik El Idrissi, B. Effect of physical and chemical parameters on the β-Tricalcium phosphate synthesized by the wet chemical method. *Med. Journal of Cem* **2018**, *7*, https://doi.org/10.13171/mjc7310268-elidrissi.